ARCHIVE OF MECHANICAL ENGINEERING

DOI: 10.24425/ame.2025.153734 2025, Vol. 72, No. 1, pp. 153–175

Agus SUSANTO [1], Budi SETIYANA [2], Rifky ISMAIL [2], Ramadhana Eka WICAKSANA [3]

Application of low-cost dynamometer based on full octagonal ring for turning process monitoring

Received 24 October 2024, **Revised** 5 January 2025, **Accepted** 23 January 2025, **Published online** 16 February 2025

Keywords: low-cost dynamometer, turning process monitoring, cutting forces, signal processing tolls

This article discusses a low-cost dynamometer based on a novel full octagonal ring-shaped transducer applied to measure the cutting forces and analyze them with the use of signal processing tools, in order determine their compatibility and the potential to monitoring machining conditions. The results showed that the performance of the developed dynamometer was in good agreement with cutting forces simulation. The cutting forces were about 30 N in stable cutting and 80 N in unstable cutting. In stable cutting, the spectrum showed the spindle frequency f_s of 5.33 Hz, corresponding to 320 rpm of spindle speed, which was followed by its harmonic frequencies of 10.66, 16 and 21.33 Hz. Revealing of all characteristic frequencies during turning processes through the frequency spectrum showed the evidence that the developed dynamometer indeed functioned well measuring cutting forces in machining. Apart of the spindle frequency of 7.5 Hz and its harmonics, there also appeared the chatter frequency f_c of 62 Hz in unstable cutting condition. By using the combination of signal processing tolls of the ensemble empirical mode decomposition with the short-time Fourier transform (EEMD-STFT), the chatter frequency was clearly captured. The combination of cutting forces measured by the developed dynamometer with EEMD-STFT makes it easier for the operator to reveal the machining conditions within a relatively short time.

✉ Agus SUSANTO, e-mail: agus_eng.dept@pnm.ac.id

[1]Laboratory of Precision Engineering, Faculty of Engineering, State Polytechnic of Madiun, Indonesia

[2]Department of Mechanical Engineering, Faculty of Engineering, Diponegoro University, Indonesia

[3]Department of Mechanical Engineering, Skoda Transportation, Czech Republic

1. Introduction

One of the machining processes widely applied in manufacturing chains is turning. This process is often applied for processing components in railway [1, 2], automotive [3–5], aerospace [6] and other industries [7, 8], especially in the stages of roughing and finishing. During the cutting process, the cutter-workpiece continuous contact produces cutting forces that are influenced by machining parameters and mechanical properties of the material [9–11]. These forces are generally measured using a table dynamometer that is installed on the tool-post of the lathe machine [12, 13]. Another way is attaching a rotating dynamometer in the spindle [14]. The forces are then analyzed for monitoring the quality of the cutting states [15], designing a machine tool [16], cutting process optimization [17], investigation in the fundamental studies of cutting tools performance [18], surface roughness evaluation [19], tool wear monitoring [20], and prediction and controlling of the chatter [21, 22].

A commercial piezoelectric dynamometer is widely utilized as a measurement instrument for quantifying the forces in order to evaluate machining process. Zheng et al. [23] used a dynamometer of Kistler 9257B placed on the tool-post of CA6240 lathe for measuring cutting forces to evaluate the Titanium Alloy turning process. Yang et al. [24] employed the same instrument for acquiring cutting forces during hard turning of nickel-based superalloy to monitor the tool wear and machining performance. Xi et al. measured cutting forces using a dynamometer for developing a tool wear monitoring system in machining process. The dynamometer was connected to the vision of the internet of production [25]. Hakmi et al. [26] used a Kistler piezoelectric dynamometer (model 9257B) for measuring cutting forces during turning polyoxymethylene (POM-C) under various cutting conditions.

However, the commercial piezoelectric dynamometer is fairly expensive. On the other hand, manufacturing processes require not only time efficiency and high reliability, but also low production costs [27]. Therefore, application of low-cost dynamometer-based cutting forces measurement may be necessary. Some researchers tried to develop a less expensive dynamometer that could be used for machining process purposes. Rizal et al. [28], Zhao et al. [29], Pathri et al. [30], Uddin et al. [31], Kumar et al. [32], Soliman [33], Dandage et al. [34] developed low-cost dynamometers based on an octagonal ring transducer to measure cutting forces in the oblique cutting process. Various transducer models were applied as an essential element of the dynamometer, including diaphragm-shaped type [35], flexible body [36], flexural beam [37, 38], hexagonal-formed ring [39], square ring [40], and two extended octagonal rings [41].

The researches shows that one of the most important components in constructing a dynamometer is the transducer. It functions as the sensing element of cutting forces during machining. In the case of the octagonal ring transducer design, used by some researchers, the strain gauge attached on the inside of the transducer is subjected to compression under normal conditions, even when the pre-compression

load has not been applied. This clearly affects the accuracy of cutting force measurements during machining operation. Therefore, alternative transducer designs need to be studied that allow for measuring the cutting forces in turning process more precisely.

Many researchers have developed low-cost dynamometers and tested them in machining tests for evaluating their performance in measuring cutting forces. Unfortunately, these dynamometers were not applied for machining process monitoring, to the best knowledge of the authors of this work.

This article describes an originally developed dynamometer based on a novel full octagonal ring-shaped transducer applied to measure the cutting forces. Signal processing tools are then used to analyze them to monitor machining process conditions.

2. Cutting forces model during turning process

The turning process allows for producing cylindrical workpieces, of both external and internal cylindrical forms. In turning, a rotating workpiece that is clamped by jaws on the spindle of the lathe machine is cut using an inserted sharp cutting tool to a certain axial cutting dept, a, as shown in Fig. 1a. This process generates the main cutting force, F, and results in producing chips. The force can then be decomposed into normal, F_x, and tangential, F_y, components, depending on the cutting angle β. These cutting forces are then transferred to the transducer and cause it to deform in two directions of x and y, as shown in Fig. 1b. The transducer then senses the forces and the dynamometer measures them.

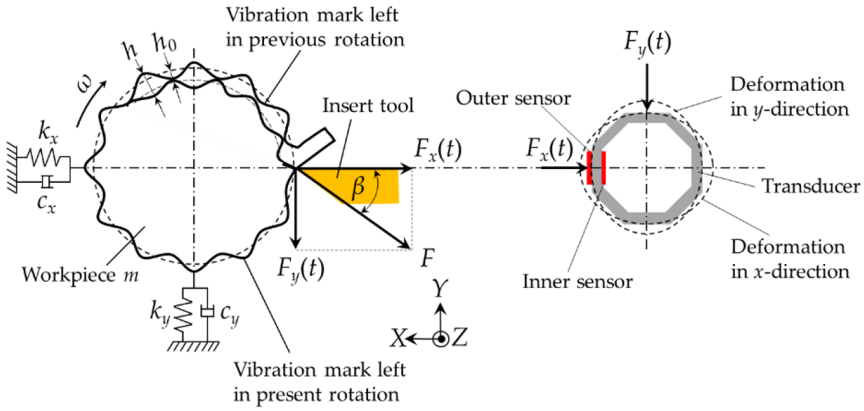

(a) cutting force modelling (b) deformation on transducer

Fig. 1. Cutting forces causing deformation on the developed transducer during turning operation

The main cutting force, F, acting during the turning process is proportional to the specific cutting force K_s (N/mm^2) multiplied by the chip cross section area

A (mm^2) according to the formula [42]:

$$F = A\,K_s. \tag{1}$$

So that, the normal and tangential cutting forces showed in Fig. 1 can be determined, $F_x = a\,h\,K_s\sin(\beta)$ and $F_y = a\,h\,K_s\cos(\beta)$. Here h is chip thickness.

On the other hand, the forces cause the workpiece to deform in the x and y directions. This is because the considered machining system is represented by flexible dynamic parameters; mass-damping-stiffness or $m{-}c{-}k$ combination. Vibrations can occur in the system, caused by main force during the chips removal. The equation of motion for a two-way oscillation system depicted in Fig. 1a can be expressed as follows:

$$[M]\begin{Bmatrix}\ddot{x}\\ \ddot{y}\end{Bmatrix}(t) + [C]\begin{Bmatrix}\dot{x}\\ \dot{y}\end{Bmatrix}(t) + [K]\begin{Bmatrix}x\\ y\end{Bmatrix}(t) = F(t), \tag{2}$$

where $[M]$, $[C]$, and $[K]$ are matrices of mass, damping coefficient, and stiffness constant, x and y are the displacements, $\dot{x}$ and $\dot{y}$ are the velocities, and time derivatives of velocities $\ddot{x}$ and $\ddot{y}$ are the accelerations in respective directions.

The deformation of the workpiece causes vibrations that are imprinted on the workpiece in the form of wavy profiles that remain after the previous period of rotation. In the next period of spindle rotation, the cutting edge of the cutter is then facing the wavy profile of the workpiece causing fluctuation of the chip thickness which becomes a function of time ($h(t)$). The phase angle difference between vibration from the previous rotation period and the current period determines the dynamic chip thickness, which then decides whether the cutting state is stable or in chattering condition. The Laplace form of the dynamic chip thickness equation is [43];

$$h(s) = h_o(s) + (e^{-s\tau} - 1)\begin{Bmatrix}x(s)\\ y(s)\end{Bmatrix}, \tag{3}$$

where h_o is the determined chip thickness and τ is the period of spindle rotation.

The frequency response function (FRF) or $[G(s)]$ can be expressed by combining the force and the displacement, namely

$$[G(s)] = \frac{1}{AK_s h(s)}\begin{Bmatrix}x(s)\\ y(s)\end{Bmatrix}. \tag{4}$$

By substituting $[G(s)]$ in Eq. (4) into Eq. (3), the ratio of the determined chip thickness to the dynamic chip thickness can be written as

$$\frac{h_o(s)}{h(s)} = \frac{1}{1 - (e^{-s\tau} - 1)\,[G(s)]\,AK_s}. \tag{5}$$

The stability limit for chatter-free machining at the chatter frequency ω_c can be given as

$$A_{\text{lim}} = -\frac{1}{2K_s \text{Re}[G(j\omega_c)]}. \tag{6}$$

By using the frequency ratio of $r = \omega/\omega_c$ and other measured dynamic modal parameters, the complex FRF in Eq. (6) can be expressed in the form of three main parts, namely the real and imaginary part of FRF, and the phase angle, as in Eq. (7), (8), and (9), respectively.

$$\text{Re}\left[G\left(\omega_c\right)\right] = \frac{1}{k}\left(\frac{1-r^2}{\left(1-r^2\right)^2 + (2\zeta r)^2}\right), \tag{7}$$

$$\text{Im}\left[G\left(\omega_c\right)\right] = \frac{1}{k}\left(\frac{-2\zeta r}{\left(1-r^2\right)^2 + (2\zeta r)^2}\right), \tag{8}$$

$$\varepsilon = \pi - 2\tan^{-1}\left(\frac{\text{Re}[G(\omega_c)]}{\text{Im}[G(\omega_c)]}\right). \tag{9}$$

Using Eqs. (6)–(9), one can draw a chart of machining stability for an arbitrary number of lobes.

3. Research methods

3.1. Construction of low-cost dynamometer and its data acquisition system

In this research, the authors developed a low-cost dynamometer and a data acquisition system which was used for measuring cutting forces and analyzed them in order to monitor the machining process states. In the developed dynamometer, a full octagonal-shaped ring, shown in Fig. 2, was applied. The dimensions of the transducer, the width, thickness, and radius of the ring were 15, 3, and 13.5 mm, respectively. The material used to produce the transducer was steel, whose material properties are summarized in Table 1.

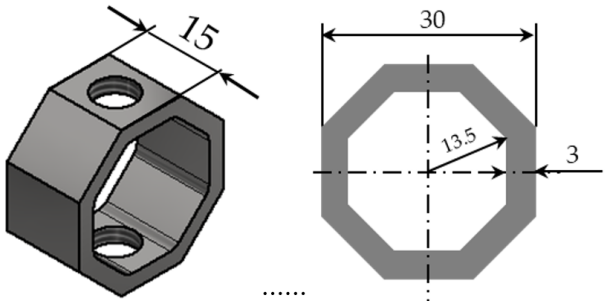

Fig. 2. The proposed transducer used in developed of dynamometer

Table 1. Material properties of steel [9]

Mechanical properties	Value
Elongation in 50 mm (l)	65-2%
Ultimate tensile strength (σ_{ul})	400–550 MPa
Yield strength (γ)	250 MPa
Young's modulus of elasticity (E)	200 GPa

The inner surface of the proposed transducer is flat, as shown Fig. 2. So that, the inner surface does not exert precompression on the sensor attached to it (the inner sensor), as shown in Fig. 1b, so the precision of cutting force measurement is improved. Besides, the sensor can be attached to the inner surface of the transducer without applying a force, which would affect the accuracy of cutting force measurement during the cutting process. On the contrary, in the previously used octagonal-elliptical-shaped ring transducer proposed by Rizal, et al. [28], Mohanraj, et al. [44], Korkut [45], Yaldiz [46, 47], Soliman [33], and others [30, 34], the sensor attached to the inner surface of the transducer is pre-compressed even when the load is not applied.

In order to characterize the strength of the proposed transducer against static loads, the Finite Element Method (FEM)-based simulation was applied. Fig. 3 shows the distribution of stresses and the safety factors of a full octagonal ring-shaped transducer subjected to normal force (F_x) and tangential force (F_y) of 224 N and 388 N. These forces were calculated by assuming the specific cutting force (K_s) of 2800 N/mm^2, the cutting angle (β) of 60°, and the feeding rate (f) of 0.2 mm/rev.

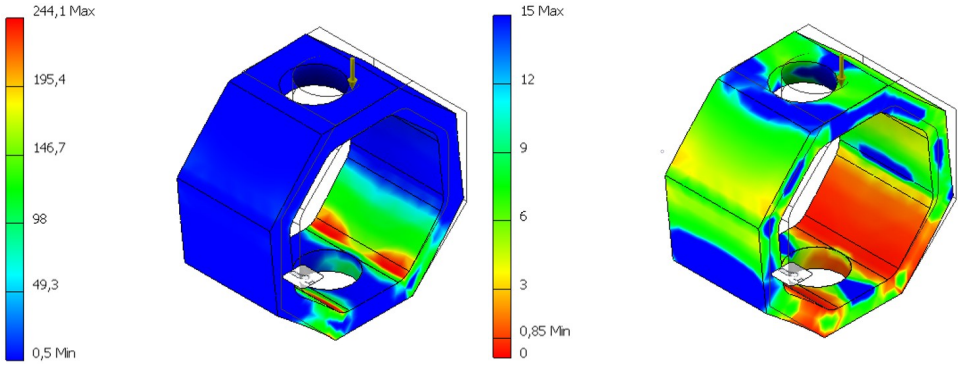

(a) distribution of stresses (MPa) (b) distribution of safety factors

Fig. 3. Condition of the transducer subjected to normal force (F_n) and tangential force (F_t) of 224 N and 388 N

The stress distribution in Fig. 3a shows stresses ranging from 0.5 to 244 MPa. The part of the transducer mark red denotes the highest stress value for the applied loads. Fig. 3b shows the safety factor of the transducer indicating that the transducer

is still in the safe condition. This is because, for the applied load, the maximum stress does not reach the yield strength of the material (γ = 250 MPa).

Fig. 4 shows the developed low-cost dynamometer and its data acquisition instruments. The dynamometer consists of four transducers placed between the top plate and the bottom plate clamped to both plates using bolt-nut of M8 size. The top plate is used to attach the cutting tool during the turning process, and the bottom plate is for connecting the dynamometer to the tool post of the machine. The other parts are data acquisition instruments consisting of a 24 V power supply, step down, an amplifier, and the ESP 32 data acquisition card. This part is usually omitted in development of a low-cost dynamometer based on previous research [28, 29, 48].

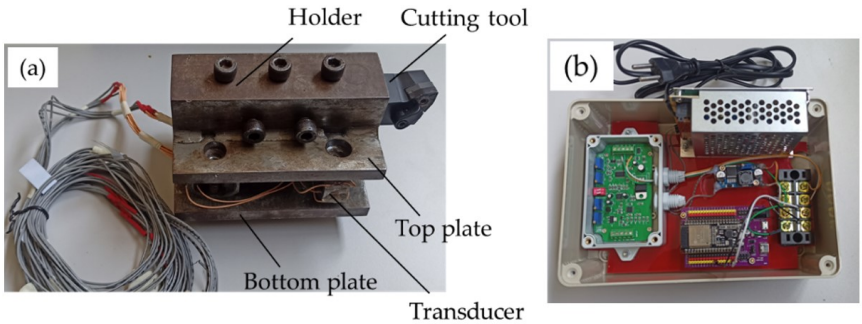

(a) parts of dynamometer (b) acquisition data instruments

Fig. 4. The developed low-cost dynamometer

3.2. Dynamometer calibrations

The calibration was performed to determine the characteristics of the dynamometer with respect to the loads applied. Schematic diagram of dynamometer calibration is shown in Fig. 5. The instruments required for the calibration included: the constructed dynamometer, the calibration test rig, the wire sling, the load, the

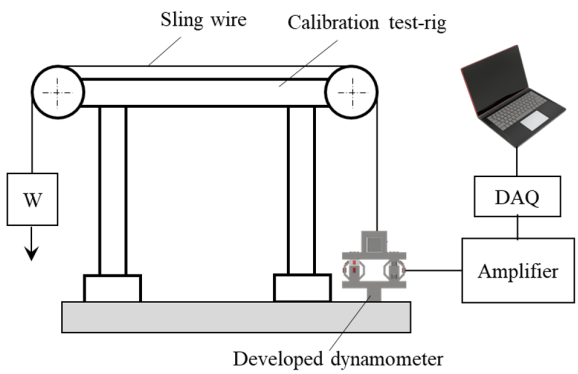

Fig. 5. Schematic diagram of dynamometer calibration

data acquisition system (DAQ), and a PC laptop computer. In the calibration, the test was carried out in two orientations of the force components, normal and tangential, with the load gradually increasing until it reached 100 N with a load step of 10 N. The results of the calibration test were also used to evaluate cross-sensitivity and linearity errors. A linear equation of force vs. voltage was obtained based on the calibration.

The results of the dynamometer calibration depicted in Figs. 6 and 7. Figs. 6a and 7a show the direct-load calibrations, which are the normal response to normal load, and the tangential response to tangential load, respectively. Figs. 6b and 7b are the cross-load calibrations, namely the normal response due to tangential load, and the tangential response caused by normal load.

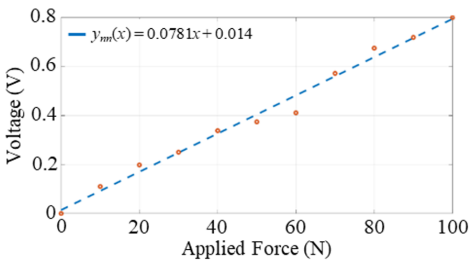

(a) direct-load calibration for normal response to normal load

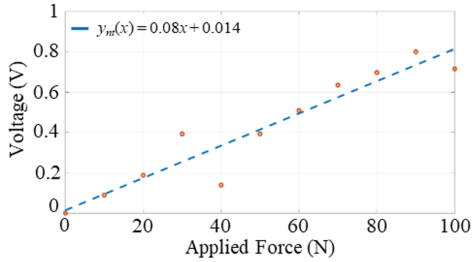

(b) cross-load calibration for normal response to tangential load

Fig. 6. Dynamometer calibration graph

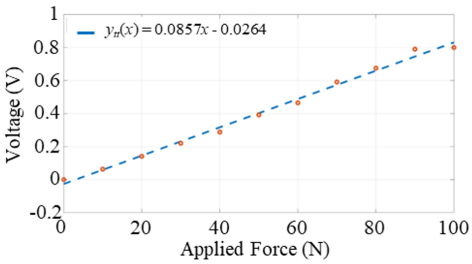

(a) direct-load calibration for tangential response to tangential load

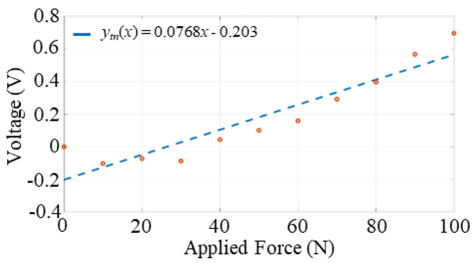

(b) cross-load calibration for tangential response to normal load

Fig. 7. Dynamometer calibration graph

The regression equation for the data in Fig. 6a is $y_{nn}(x) = 0.0781x + 0.014$ with an RMSE of 2.9%, and an MAE of 2.1%. While, the dynamometer sensitivity due to this calibration is 78.1 mV/N. Fig. 6b shows the calibration of the normal force dynamometer to tangential loading. The regression equation in this case is $y_{nt}(x) = 0.08x + 0.014$ with an RMSE and MAE of 0.8% and 0.6%, respectively. When a maximum load of about 100 N was applied to the dynamometer, the cross-

sensitivity of the developed dynamometer reached 10.2% and the linearity error was 0.63%.

Fig. 7a shows an upward data trend with a regression equation of $y_{tt}(x) = 0.0857x - 0.0264$ with an RMSE of 2.3% and an MAE of 1.9%. The sensitivity of the tangential force dynamometer is 85.7 mV/N. The tangential force dynamometer calibration due to normal loading is shown in Fig. 7b. The regression equation for the data is $y_{tn}(x) = 0.0077x - 0.0203$ with an RMSE of 0.9% and an MAE of 0.8%. The cross-sensitivity and linearity error of these calibrations are 8.98% and 3.7%, respectively.

3.3. Identification of cutting system dynamics

The identification of the dynamics of the cutting system was carried out through impact tests in order to measure the frequency response functions (FRFs). Dynamic modal parameters were then extracted by modal analysis technique, similarly as it has been applied in various fields, including dynamics analysis of automotive body [49, 50], milling structure [51], and others. The impact test experiment on the workpiece-spindle combination is depicted in Fig. 8. The Dytran-5800B3 piezoelectric hammer was applied to excite the structure. The impulse force of the hammer was measured by a sensor mounted on the hammer tip and its free vibration response was measured by a Dytran-3413A2 accelerometer attached to the workpiece tip. Both impulse and response were registered using a GW Instek oscilloscope. The way of hitting the structure to obtain direct FRFs in the x and y directions is illustrated Figs. 8b and 8c.

The FRFs obtained from the experiments are shown in Fig. 9. They consist of real and imaginary parts of FRFs, $G_{xx}(\omega)$ and $G_{yy}(\omega)$, which are represented in black and red curves, respectively. The FRFs have been marked with various points including the natural frequency (f_n) corresponding to the receptance magnitude (A), and two specific frequencies f_a and f_b. Based on these variables, the dynamic parameters could be determined using modal analysis technique. The results are tabulated in Table 2.

Table 2. Dynamic modal parameters of cutting system associated with Fig. 8

Direction of FRF	Modal mass, m, kg	Damping coefficient, c, N s/m	Stiffness constant, k, N/m	Damping ratio, ζ, (%)	Natural frequency, f_n, Hz
$G_{xx}(\omega)$	0.052	60	2.7×10^6	1.26	61
$G_{yy}(\omega)$	0.047	50	2.5×10^6	1.75	60

As explained in Section 2, the machining stability diagram can then be produced based on these dynamic parameters and assuming the cutting force coefficient, K_s, of 2600 N/m^2 for 1045 carbon steel material [42]. The results are shown in Fig. 10, which depicts stability chart with eight lobes for spindle speeds ranging from 0 to 1000 rpm.

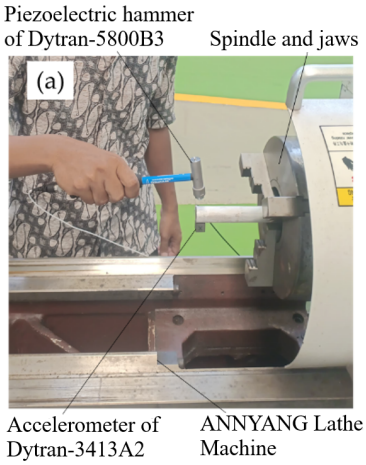

(a) experimental setup

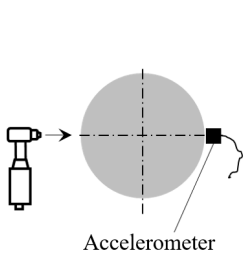

(b) impact method to determine direct FRFs in x direction

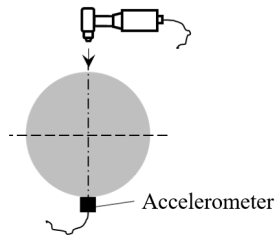

(c) impact method to determine direct FRFs in y direction

Fig. 8. Hammering test to identify dynamic cutting system

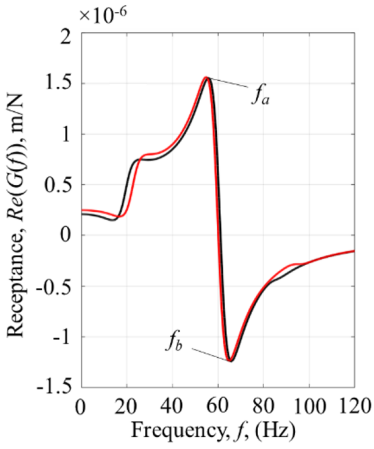

(a) real part of FRF

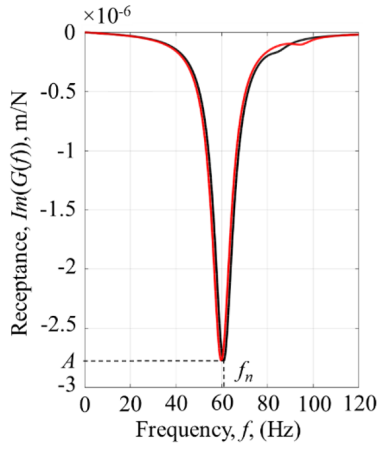

(b) imaginary part of FRFs

Fig. 9. FRFs obtained from the experiments

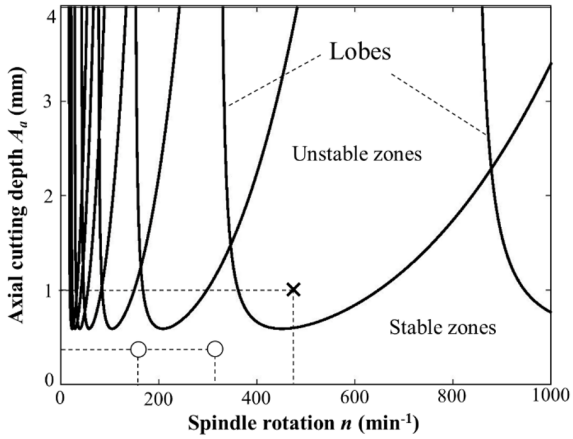

Fig. 10. Stability chart for determining turning process parameters

3.4. Experimental cutting tests

To evaluate the performance of the developed dynamometer used for machining process monitoring, experimental cutting tests were carried out. Fig. 11 shows an experimental setup for turning process to measure cutting forces using the developed dynamometer. A workpiece of AISI 1045 with 25.4 mm in diameter and 100 mm in length was clamped by an independent three-jaw chuck on the spindle machine. This type of material is often applied as mechanical components in industries. As can be seen from the figure, tool holder DASAN MWLNR (20 × 20 mm) with tungsten carbide insert cutting tool (WNMG0804) placed on the developed dynamometer with fixed tool-overhang and clamped with M8 bolts placed on the lathe tool-post. Thus, this developed dynamometer was easier to use compared to cutting force measurements using a piezoelectric-based table dynamometer which had been generally used [12, 25, 52]. This is because the installation does not require dismantling the lathe tool post.

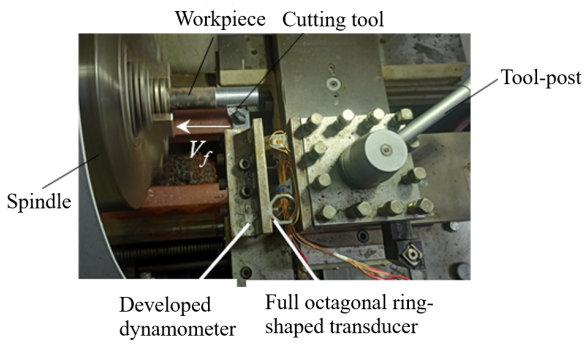

Fig. 11. Experimental setup in turning process using developed dynamometer

In the experimental tests, the rotating workpiece was cut by a carbide insert cutting tool at a feed rate f = 0.06 mm/rev, and other machining parameters were determined based on the diagram shown in Fig. 10. From there, tests were carried out under stable conditions using combinations of axial depth of cut A_a = 0.2 mm and spindle rotational speed n = 160 rpm, and A_a = 0.2 mm and n = 320 rpm. Another test was a combination of axial depth of cut A_a = 1 mm and spindle rotational speed n = 450 rpm under unstable conditions. The machining parameters are summarized in Table 3.

Table 3. Machining parameters used in cutting tests

Spindle rotational speed, n (rpm)	Feed rate, f (mm/rev)	Axial depth of cut, A_a (mm)	Machining condition
160	0.06	0.2	Stable
320	0.06	0.2	Stable
450	0.06	1	Unstable

4. Results and discussions

4.1. Performance of the developed dynamometer assessed by experimental cutting

The cutting forces obtained from the experimental turning process are shown in Fig. 12. These cutting forces are associated to machining parameters of axial cutting depth of A_a = 0.2 mm with a spindle rotational speed of n = 160 rpm in stable conditions. The cutting time corresponded to given machining parameters with about 50 mm of cutting length. Blue and green colors of the graphs represent

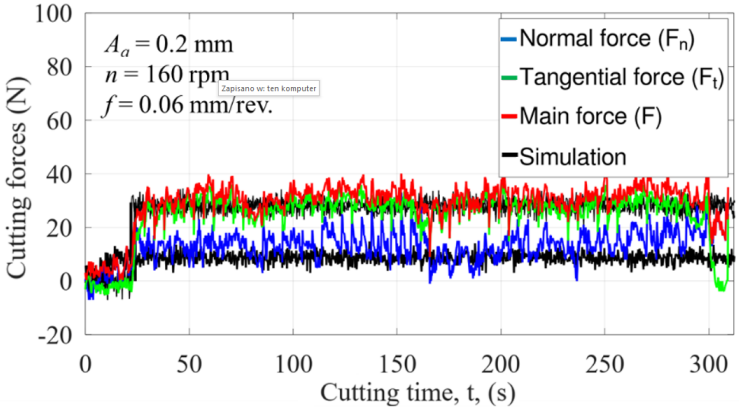

Fig. 12. Cutting forces measured from turning tests comparing to the simulation using given machining parameters in stable condition

the normal and tangential cutting forces, respectively. The red one is the main cutting force, the resultant of the two cutting forces calculated as $F = \sqrt{F_x^2 + F_y^2}$. The black one is the simulation cutting force determined with formulas given in Section 2 with random noise added in the simulations. It is because fluctuation of the cutting forces is caused by many effects occurring during continuous contact between the workpiece and the cutter, the noise originating from the surrounding environment [53–55] and other random effects that should not be ignored [56].

The comparison presented in Fig. 12 indicates that the measured cutting forces are in good agreement with the simulation ones. Besides, these cutting forces trend to have similar trends as those from the previous studies, in which commercial piezoelectric dynamometers were used [37, 57, 58]. This indicates that the developed dynamometer is acceptable for measuring cutting forces in turning processes, although the frequency characteristics of the cutting forces still needs to be examined, which will be the subject of the following discussion.

4.2. Cutting forces analysis for machining stability monitoring

Fig. 13 shows the cutting forces acquired in cutting tests based on the predetermined machining conditions. Fig. 13a depicts cutting forces acquired in a stable operation. They appear to be consistent with analytical predictions based on the stability diagram shown in Fig. 10. With the machining parameters of $n = 320$ rpm and axial cutting depth of $A_a = 0.2$ mm, the cutting process is clearly in a stable state. Besides, the cutting time is shorter compared to that of the first experiment, as shown in Fig. 12. The magnitude of cutting forces does not depend on the spindle rotational speed, but it depends on the cutting time.

In Fig. 13b there are presented the cutting forces measured during unstable machining. As can be seen from this figure, the magnitudes of forces are growing significantly and become larger than those in Fig. 13a. The main cutting force in Fig. 13a is about 35 N and the main cutting force in Fig. 13b is about 75 N. Here, the cutting force was indeed influenced by the cutting dept [42].

To determine the effect of machining parameters on the characteristics of the turning process, it is necessary to transform the measured forces displayed in Fig. 13 into frequency spectra to examine the frequency contents of the forces. The frequency spectra calculated by the fast Fourier transform are shown in Fig. 14.

The spectra above show the frequency content of the cutting forces, both normal, tangential, and main cutting forces, which are denoted with the color of each graph. As can be seen in the frequency spectra above, there are various frequencies that can be distinguished, including the spindle rotational frequency (f_s) and its harmonic frequencies marked by the arrows. Both the fundamental spindle frequency and its harmonics are the characteristic frequencies resulting from the spindle rotational speed. According to the frequency spectrum in Fig. 14a, the spindle rotational frequency equals 5.33 Hz. It is associated with the spindle

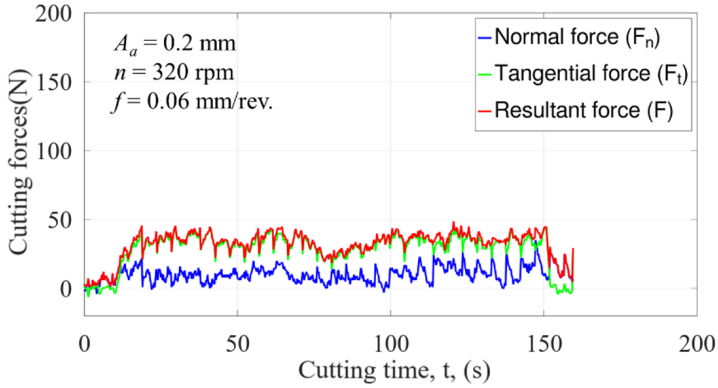

(a) Stable machining using assumed machining parameters

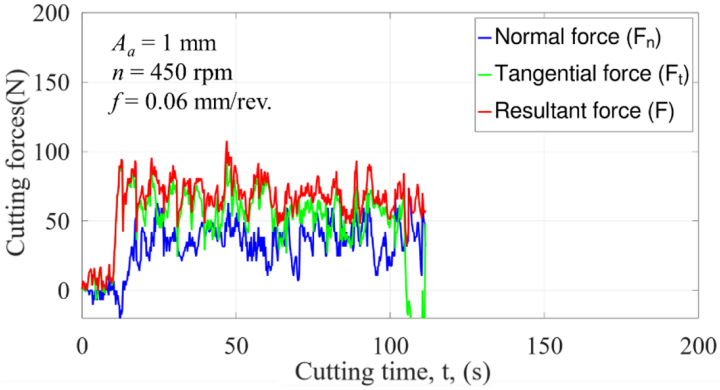

(b) Unstable machining using assumed machining parameters

Fig. 13. Cutting forces obtained from experimental turning tests compared to the simulation using assumed machining parameters in stable condition

rotation speed of n = 320 rpm used in machining. This frequency is followed by harmonic frequencies, namely 10.66, 16; 21.33 Hz and so on. All of these characteristic frequencies are of force vibrational type. These characteristic frequencies of the cutting process, determined through the frequency spectrum above, provide yet another evidence that the developed dynamometer actually functions well, and is suitable to measure cutting forces in the turning process. On the other hand, Fig. 14b shows the spindle frequency f_s at 7.5 Hz and its harmonic frequencies which are associated with spindle rotational speed of n = 450 rpm. In addition, a more subtle observation of this spectrum allows us to see the chatter frequency (f_c = 62 Hz). The chatter generally arises near the natural frequency of the cutting system [51, 59, 60].

In order to make the monitoring of machining process clearer, the digital signal processing tools of the Ensemble Empirical Mode Decomposition (EEMD) were applied in conjunction with the short-time Fourier transform (STFT). Ordinarily,

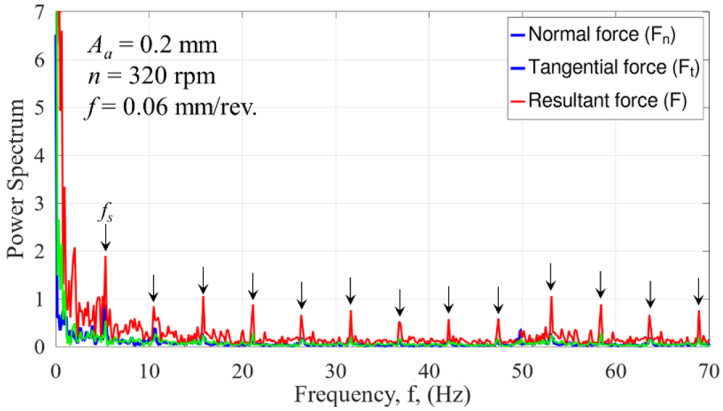

(a) Stable machining

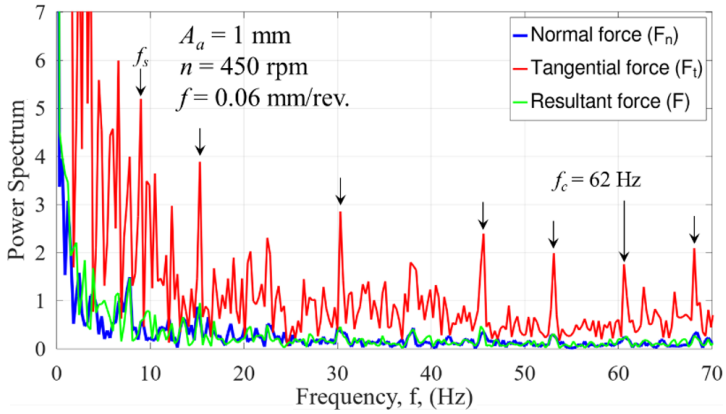

(b) Unstable machining

Fig. 14. Frequency spectrum corresponding to the cutting forces obtained in cutting test

EEMD is used together with the Hilbert transform (HT) to reveal abnormality phenomena in many mechanical systems, such as chatter detection in milling processes [58], cutting tools breakages [63], bearing faults [64], and diesel engine instability detections [65]. This is because EEMD and HT are two consecutive steps in implementing the Hilbert-Huang transform (HHT) [66]. EEMD function is to decompose any complex signal into simple components called the intrinsic mode functions (IMFs). HT is then used to plot the IMF components on one time-frequency plane. However, high computation load is the weakness of HHT [67, 68]. Therefore, its application in machining process monitoring may be quite time-consuming. Therefore, the combination EEMD-STFT is a possible step used in practice to monitor the machining process conditions quickly.

A set of IMFs in time domain processed by the EEMD is shown in Figs. 15 and 16, which correspond to stable and unstable main cutting forces, respectively.

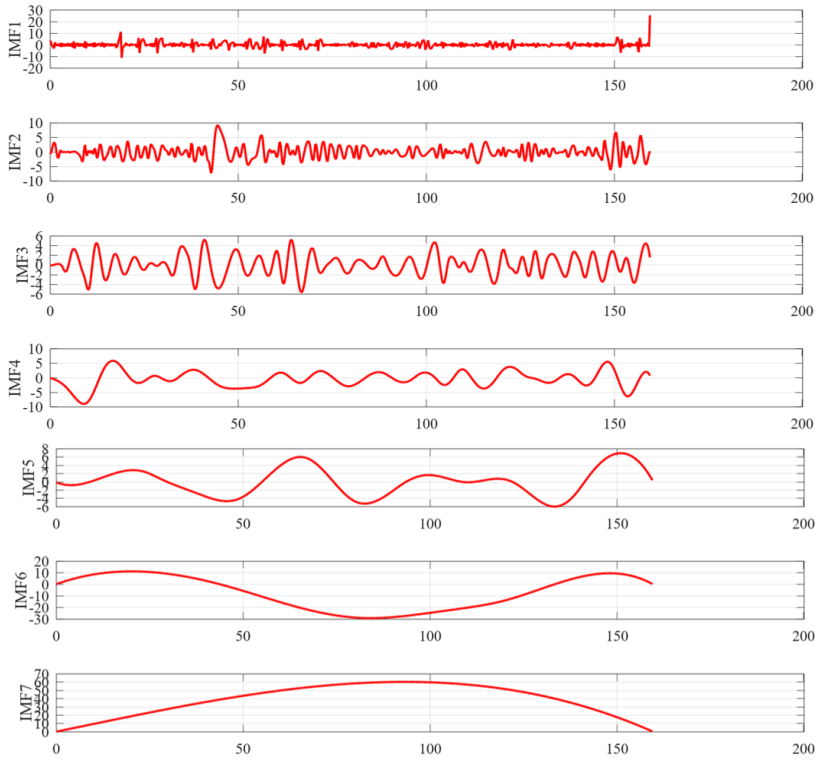

Fig. 15. Decomposed signal for stable force corresponding to raw signal in Fig. 13a

The decomposition process has been explained in the paper [67]. EEMD has a unique principle of working, namely separating data that have complex frequencies into simple frequencies. From Figs. 15 and 16, it can be seen that IMF1 contains most of the oscillations, which means that it has the highest frequency among the other IMFs. The last one is process residue which has no meaning because there isn't even one oscillation.

The next step is transforming the IMF into a spectrum in the time-frequency domain using STFT. The resulting spectrum is shown in Fig. 17. Figs. 17a and 17b are the STFT spectra for stable and unstable machining, respectively. According to these spectra, in stable machining, the level of energy spread in the STFT window is low. On the contrary, the energy level of unstable machining, which is shown in the second STFT spectrum, increases and is concentrated at the chatter frequency.. The time required to generate all the spectra was relatively short, approximately about three seconds. This would certainly make it easier for the operators to examine the condition of the machining process they are handling, for example processing automotive and railway shaft components. This confirms that EEMD-STFT has the ability to reveal the current state of turning operation based on the cutting force obtained using given cutting parameters.

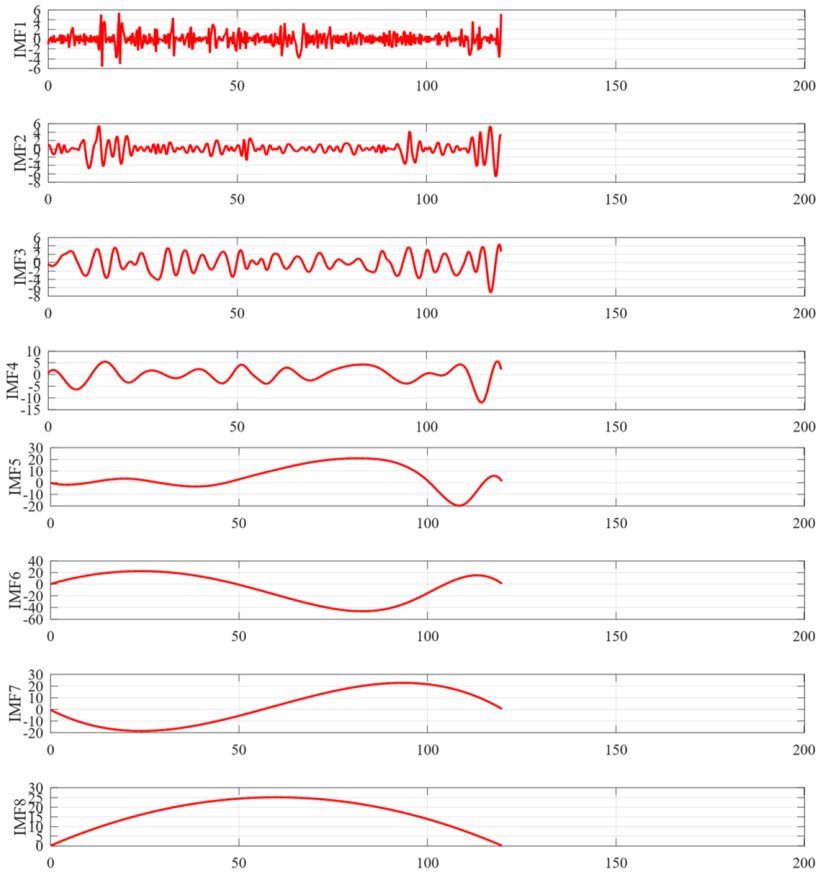

Fig. 16. Decomposed signal for unstable force corresponding to raw signal in Fig. 13b

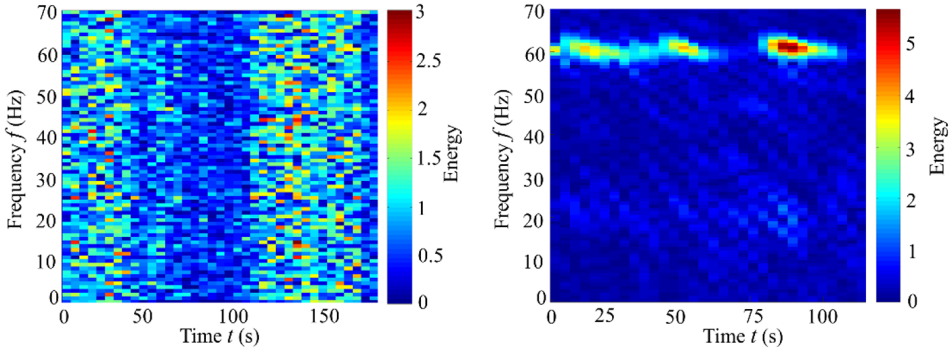

(a) STFT spectra correspond to stable machining

(b) STFT spectra correspond to stable machining

Fig. 17. STFT spectra used for turning process monitoring

This result can be confirmed based on the images of the machined surface produced during machining process, as shown in Fig. 1. The machined surface obtained in a stable process, Fig. 18a, shows that there is no mark of chatter on the surface of workpiece. The reasonable surface roughness in this product might be explained by the fact that the instability of sliding contact between the tool and the workpiece depends only on the fluctuations of friction coefficient during sliding, not on the chatter vibrations [69, 70]. Fig. 18b shows the chatter that was imprinted on the surface of the workpiece.

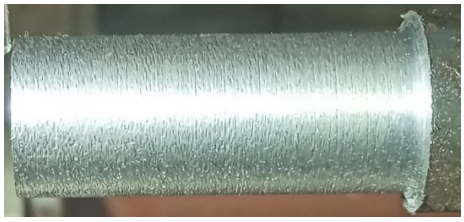

(a) Smooth surface of workpiece

(b) Chatter imprinted on workpiece surface

Fig. 18. Machined surfaces generated in turning tests

5. Conclusions

A low-cost dynamometer has been developed for measuring cutting force during turning process and it has been validated by calibration and simulation. Based on the presented results and discussions, some important conclusions can be drawn:

1. The developed dynamometer indeed performed well in measuring cutting forces during turning processes and provided good agreement between the measures cutting forces and the simulation.
2. The characteristic frequencies of the turning process determined through frequency analysis, which include the frequency of rotational spindle speed and its harmonic frequencies, show another evidence that the developed dynamometer works properly.
3. In turning process monitoring by analyzing the cutting forces, unstable conditions during the machining process can be distinguished from the stable ones. Frequency chatter appears at 62 Hz in the frequency spectrum of forces in unstable conditions, according to the frequency spectrum calculated by fast Fourier transform (FFT).
4. The machining process conditions can be easily and clearly recognized in time-frequency domain using the combination of EEMD-STFT. The short time of cutting force analysis using that signal processing tool will also make it easier for operators to recognize machining process conditions.
5. The cutting forces measured using the developed dynamometer are compatible with the signal processing tools of EEMD-STFT.

References

[1] Sandvik Coromant: Railway turning: Railway turning: Re-turning and new wheel turning. Application Guide, 2022.

[2] Korloy Railway Industry. Technical Information KORLOY: Railway Industry, 2022.

[3] N. Sultana and N.R. Dhar. Hybrid GRA-PCA and modified weighted TOPSIS coupled with Taguchi for multi-response process parameter optimization in turning AISI 1040 steel. *Archive of Mechanical Engineering*, 68(1):23–49, 2021. doi: 10.24425/ame.2020.131707.

[4] A. Hamdi, S.M. Merghache, and T. Aliouane, Effect of cutting variables on bearing area curve parameters (BAC-P) during hard turning process. *Archive of Mechanical Engineering*, 67(1):73–95, 2020. doi: 10.24425/ame.2020.131684.

[5] K. Zak. Cutting mechanics and surface finish for turning with differently shaped CBN tools. *Archive of Mechanical Engineering*, 64(3):347–357, 2017. doi: 10.1515/meceng-2017-0021.

[6] D. Shi and N.N. Gindy. Development of an online machining process monitoring system: Application in hard turning. *Sensors and Actuators A: Physical*, 135(2):405–414, 2007. doi: 10.1016/ j.sna.2006.08.011.

[7] J. Lukács and R. Horváth. Comprehensive investigations of cutting with round insert: introduction of a predictive force model with verification. *Metals*, 12(2):257, 2022. doi: 10.3390/met12020257.

[8] M. Mudjijanto, Sulistyo, and R. Rusnaldy. Analysis of chip geometry and surface roughness at low speed turning in various commercial steels. *MATEC Web of Conferences*, 159:02018, 2018. doi: 10.1051/matecconf/201815902018.

[9] S. Kalpakjian and S.R. Schmid. *Manufacturing Engineering and Technology*. Prentice Hall, 2001.

[10] G. Tlusty. *Manufacturing Processes and Equipment*. Practice-Hall, 2020.

[11] H. Li and Y. Chen. *Handbook of Manufacturing Engineering and Technology*. Springer-Verlag, 2014.

[12] K. Zhuang, Z. Shi, Y. Sun, Z. Gao, and L. Wang. Digital twin-driven tool wear monitoring and predicting method for the turning process. *Symmetry*, 13(8):1438, 2021. doi: 10.3390/sym13081438.

[13] S. Krajcoviech, J. Holubjak, M. Richtarik, and T. Czánová. Identification of process Prime A turning when machining steel C56E2 and monitoring of cutting forces. *Transportation Research Procedia*, 55:605–612, 2021. doi: 10.1016/j.trpro.2021.07.027.

[14] M. Rizal, J.A. Ghani, M.Z. Nuawi, and C.H.C. Haron. Development and testing of an integrated rotating dynamometer on tool holder for milling process. *Mechanical Systems and Signal Processing*, 52-53:559–576, 2015. doi: 10.1016/j.ymssp.2014.07.017.

[15] J.H. Kim, H.K. Chang, D.C. Han, D.Y. Jang, and S.I. Oh. Cutting force estimation by measuring spindle displacement in milling process. *CIRP Annals*, 54(1):67–70, 2005. doi: 10.1016/S0007-8506(07)60051-1.

[16] F. Cus, M. Milfelner, and J. Balic. An intelligent system for monitoring and optimization of ball-end milling process. *Journal of Materials Processing Technology*, 175(1-3):90–97, 2006. doi: 10.1016/j.jmat protec.2005.04.041.

[17] F. Cus, and J. Balic. Optimization of cutting process by GA approach. *Robotics and Computer-Integrated Manufacturing*, 19(1-2):113–121, 2003. doi: 10.1016/S0736-5845(02)00068-6.

[18] J.A. Ghani, I.A. Choudhury, and H.H. Masjuki. Performance of P10 TiN coated carbide tools when end milling AISI H13 tool steel at high cutting speed. *Journal of Materials Processing Technology*, 153-154:1062–1066, 2004. doi: 10.1016/j.jmatprotec.2004.04.353.

[19] B. Huang and J.C. Chen. An in-process neural network-based surface roughness prediction (INN-SRP) system using a dynamometer in end milling operations. *The International Journal of Advanced Manufacturing Technology* 21:339–347, 2003. doi: 10.1007/s001700300039.

[20] S.R. Agari. Wear and surface characteristics on tool performance with CVD coating of Al_2O_3/TiCN inserts during machining of Inconel 718 alloys. *Archive of Mechanical Engineering*, 69(1):59–75, 2021. doi: 10.24425/ame.2021.139647.

[21] G. Quintana, J. Ciurana, Chatter in machining processes: A review. *International Journal of Machine Tools and Manufacture*, 51(5):363–376, 2011. doi: 10.1016/j.ijmachtools.2011.01.001.

[22] P. Huang, J. Li, J. Sun, and J. Zhou. Vibration analysis in milling titanium alloy based on signal processing of cutting force. *The International Journal of Advanced Manufacturing Technology*, 64:613–621, 2013. doi: 10.1007/s00170-012-4039-x.

[23] Q. Zheng, C. Yang, S. Zhang, and Y. Hu. Simulation and experimental research on cutting force of turning titanium alloy. *MATEC Web of Conferences*, 31:03013, 2015. doi: 10.1051/matecconf/20153103013.

[24] Y. Qiao, X. Ai, and Z. Liu. Machining performance and tool wear of coated carbide inserts in high speed turning powder metallurgy nickel-base superalloy. In: *2010 WASE International Conference on Information Engineering*, pages 71–74,Beidai, China, 2010. doi: 10.1109/ICIE.2010.195.

[25] T. Xi, I.M. Beninca, S. Kehne, M. Fey, and C. Brecher, Intelligent monitoring of tool wear based on machine internal data. *WT Werkstattstech*, 111(05):309–313, 2021. doi: 10.37544/1436-4980-2021-05-43.

[26] T. Hakmi, A. Hamdi, Y. Touggui, A. Laouissi, S. Belhadi, and M.A. Yallese. Machinability investigation during turning of polyoxymethylene POM-C and optimization of cutting parameters using Pareto analysis, linear regression and genetic algorithm. *Archive of Mechanical Engineering*, 71(1):47–71, 2024. doi: 10.24425/ame.2024.149184.

[27] C.H. Lauro, L.C. Brandão, D. Baldo, R.A. Reis, and J.P. Davim. Monitoring and processing signal applied in machining processes – A review. *Measurement*, 58:73–86, 2014. doi: 10.1016/j.measurement.2014.08.035.

[28] M. Rizal, J.A. Ghani, Husni, and Husaini. Design and construction of a strain gauge-based dynamometer for a 3-axis cutting force measurement in turning process. *Journal of Mechanical Engineering and Sciences*, 12(4):4072–4087, 2018. doi: 10.15282/jmes.12.4.2018.07.0353.

[29] Z. You, Z. Yulong, G. Taobo. Application of a strain gauge cutting force sensor in machining process monitoring. In: *2019 14th IEEE International Conference on Electronic Measurement & Instruments (ICEMI)*, pages 891–897, Changsha, China, 2019. doi: 10.1109/ICEMI46757.2019.9101849.

[30] B.P. Pathri, A.K. Garg, D.R. Unune, H.S. Mali, S.S. Dhami, and R. Nagar. Design and fabrication of a strain gauge type 3-axis milling tool dynamometer. *International Journal of Materials Forming and Machining Processes (IJMFMP)*, 3(2):1–15, 2016. doi: 10.4018/ijmfmp.2016070101.

[31] M.S. Uddin, and D. Songyi. On the design and analysis of an octagonal-ellipse ring based cutting force measuring transducer. *Measurement*, 90:168–177, 2016. doi: 10.1016/j.measurement.2016.04.055.

[32] H. Kumar, Pardeep, M. Kaushik, and A. Kumar. Development and characterization of a modified ring shaped force transducer. *MAPAN-Journal of Metrology Society of India*, 30:37–47, 2015. doi: 10.1007/s12647-014-0118-9.

[33] E. Soliman. Performance analysis of octal rings as mechanical force transducers. *Alexandria Engineering Journal*, 54(2):155–162, 2015. doi: 10.1016/j.aej.2015.01.004.

[34] R. V Dandage, S.G. Bhatwadekar, and M.M. Bhagwat. design, development and testing of a four component milling tool dynamometer. *International Journal of Applied Engineering and Technology*, 2:45–50, 2012.

[35] R. Kumar, B.D. Pant, and S. Maji. Development and characterization of a diaphragm-shaped force transducer for static force measurement. *MAPAN-Journal of Metrology Society of India*, 32:167–174, 2017. doi: 10.1007/s12647-017-0207-7.

[36] M. Liu, Z. Zhang, Z. Zhou, S. Peng, and Y. Tan. A new method based on Fiber Bragg grating sensor for the milling force measurement. *Mechatronics*, 31:22–29, 2015. doi: 10.1016/j.mechatronics.2015.03.007.

[37] U. Şeker, A. Kurt, and I. Çiftçi. Design and construction of dynamometer for measurement of cutting forces during machining with linear motion. *Materials & Design*, 23(4):355–360, 2002. doi: 10.1016/s0261-3069(02)00013-4.

[38] Z. Xie, Y. Lu, and J. Li. Development and testing of an integrated smart tool holder for four-component cutting force measurement. *Mechanical Systems and Signal Processing*, 93:225–240, 2017. doi: 10.1016/j.ymssp.2017.01.038.

[39] H. Kumar, C. Sharma, A. Kumar, P.K. Arora, and S. Kumar. Design, development and metrological characterization of a low capacity precision industrial force transducer. *ISA Transactions*, 58:659–666, 2015. doi: 10.1016/j.isatra.2015.07.011.

[40] H. Kumar, C. Sharma, and A. Kumar. The development and characterization of a square ring shaped force transducer. *Measurement Science and Technology*, 24(9):095007, 2013. doi: 10.1088/0957-0233/ 24/9/095007.

[41] A.A. Ammar, M. Jallouli, and Z. Bouaziz. Design and development of a dynamometer for the simulation of the cutting forces in milling. *International Journal of Automation and Control*, 5(1):44–60, 2011. doi: 10.1504/ IJAAC.2011.037379.

[42] T.L. Schmitz and K.S. Smith. *Machining Dynamics: Frequency Response to Improved Productivity*, Springer, 2008.

[43] Y. Altintas. *Manufacturing Automation: Metal Cutting Mechanics, Machine Tool Vibrations, and CNC Design*. Cambridge University Press Cambridge, 2012.

[44] T. Mohanraj, T. Deepesh, R. Dhinesh, S. Jayaprakash, and S. Sai Krishna. Design and analysis of a strain gauge based eight-shaped elliptical ring dynamometer for milling force measurement. *Proceedings of the Institution of Mechanical Engineers, Part C: Journal of Mechanical Engineering Science*, 235(17):3125–3134, 2021. doi: 10.1177/0954 406220967681.

[45] I. Korkut. A dynamometer design and its construction for milling operation. *Materials & Design*, 24(8):631–637, 2023. doi: 10.1016/S0261-3069(03)00122-5.

[46] S. Yaldiz and F. Ünsaçar. Design, development and testing of a turning dynamometer for cutting force measurement. *Materials & Design*, 27(10):839–846, 2006. doi: 10.1016/j.matdes.2005.04.001.

[47] S. Yaldiz, F. Ünsaçar, H. Saglam, and H. Işik. Design, development and testing of a four-component milling dynamometer for the measurement of cutting force and torque. *Mechanical Systems and Signal Processing*, 21(3):1499–1511, 2007. doi: 10.1016/j.ymssp.2006.06.005.

[48] M. Rizal, J.A. Ghani, and A.Z. Mubarak. Design and development of a tri-axial turning dynamometer utilizing cross-beam type force transducer for fine-turning cutting force measurement. *Sensors*, 22(22):8751, 2022. doi: 10.3390/s22228751.

[49] W. Jing, Z. Hong, X. Gang, W. Erbing, and L. Xiang. Operational modal analysis for automobile. In Zhang, Y. (ed): *Future Communication, Computing, Control and Management*, pages 525–532, 2012. doi: 10.1007/978-3-642-27311-7_70.

[50] Z.M. Hafizi, A.M. Aizzuddin, N.I.A. Halim, and M.F. Jamaludin. Modal properties investigation of car body-in-white with attached windscreen and rear screen. *IOP Conference Series: Materials Science and Engineering*, 257:012038, 2017. doi: 10.1088/1757-899X/257/1/012038.

[51] Z. Zhang, H. Li, X. Liu, W. Zhang, and G. Meng. Chatter mitigation for the milling of thin-walled workpiece. *International Journal of Mechanical Sciences*, 138-138:262–271, 2018. doi: 10.1016/j.ijmecsci.2018.02.014.

[52] F.J. Amigo, G. Urbikain, L.N. López de Lacalle, O. Pereira, P. Fernández-Lucio, and A. Fernández-Valdivielso. Prediction of cutting forces including tool wear in high-feed turning of Nimonic® C-263 superalloy: A geometric distortion-based model. *Measurement*, 211:112580, 2023. doi: 10.1016/j.measurement.2023.112580.

[53] A. Susanto, K. Yamada, K. Mani, R. Tanaka, and K. Sekiya. Vibration analysis in milling of thin-walled workpieces using Hilbert-Huang transform. In: *Proceedings of International Conference on Leading Edge Manufacturing in 21st century: LEM21*, 2017, pages 1–6. doi: 10.1299/jsmelem.2017.9.031.

[54] A. Susanto, K. Yamada, R. Tanaka, M. Azka, M.P. Sekiya, and P. Novia. Analysis of transient signal using Hilbert-Huang transform for chatter monitoring in turning process. In: 2019 4th International Conference on Information Technology, Information Systems and Electrical Engineering (ICITISEE), pages 26–30, Yogyakarta, Indonesia, 2019. doi: 10.1109/ICITISEE48480.2019.9003862.

[55] A. Susanto, B. Artono, S. Khonjun, and R. Mahmud. Denoising of disturbed signal using reconstruction technique of EMD for railway bearing condition monitoring. *International Journal of Computer Science Issues (IJCSI)*, 17(5):15–22, 2020. doi: /10.5281/zenodo.4418876.

[56] A. Panda, A.K. Sahoo, R. Kumar, and D. Das. A concise review of uncertainty analysis in metal machining. *Materials Today Proceedings*, 26(2):1734–1739, 2020. doi: 10.1016/j.matpr.2020.02.365.

[57] O. Cahuc, A. Gerard, C. Bisu, and C. Ispas. A force torsor analysis for a turning process in the presence of selfexcited vibrations. *Applied Mechanics Materials*, 62:135–146, 2011. doi: 10.4028/www. scientific.net/AMM.62.135.

[58] G. Fodor, H.T. Sykora, and D. Bachrathy. Stochastic modeling of the cutting force in turning processes. *The International Journal of Advanced Manufacturing Technology*, 111:213–226, 2020. doi: 10.1007/s00170-020-05877-8.

[59] X.B. Dang, M. Wan, Y. Yang, and W.H. Zhang. Efficient prediction of varying dynamic characteristics in thin-wall milling using freedom and mode reduction methods. *International Journal of Mechanical Sciences*, 150:202–216, 2019. doi: 10.1016/j.ijmecsci.2018.10.009.

[60] A.Z. Rahman, K. Jauhari, M. Al Huda, N.A. Untariyati, M. Azka, R. Rusnaldy, and A. Widodo. Correlation analysis of vibration signal frequency with tool wear during the milling process on martensitic stainless steel material. *Arabian Journal for Science and Engineering* 49:10573–10586, 2023. doi: 10.1007/s13369-023-08397-1.

[61] S. Wan, X. Li, W. Chen, and J. Hong. Investigation on milling chatter identification at early stage with variance ratio and Hilbert–Huang transform. *The International Journal of Advanced Manufacturing Technology*, 95:3563–3573, 2018. doi: 10.1007/s00170-017-1410-y.

[62] M. Lu, B. Chen, D. Zhao, J. Zhou, J. Lin, A. Yi, and H. Wang. Chatter identification of three-dimensional elliptical vibration cutting process based on empirical mode decomposition and feature extraction. *Applied Sciences*, 9(1):21, 2019. doi: 10.3390/app9010021.

[63] T. Kalvoda and Y.R. Hwang. A cutter tool monitoring in machining process using Hilbert-Huang transform. *International Journal of Machine Tools and Manufacture*, 50(5):495–501, 2010. doi: 10.1016/j.ijmachtools. 2010.01.006.

[64] A. Lakikza, H. Cheghib, and N. Kahoul. Optimized variational mode decomposition for improved bearing fault diagnosis and performance evaluation. *Arch. Mech. Eng.*, 71(4):467–495, 2024. doi: 10.24425/ame.2024.152615.

[65] Y.S. Wang, Q.H. Ma, Q. Zhu, X.T. Liu, and L.H. Zhao. An intelligent approach for engine fault diagnosis based on Hilbert – Huang transform and support vector machine. *Applied Acoustics*, 75:1–9, 2014. doi: 10.1016/j.apacoust.2013.07.001.

[66] N.E. Huang and S.S.P. Shen. *Hilbert–Huang Transform and Its Applications*. World Scientific Publishing, 2005.

[67] A. Susanto, C.H. Liu, K. Yamada, Y.R. Hwang, R. Tanaka, and K. Sekiya. Application of Hilbert–Huang transform for vibration signal analysis in end-milling. *Precision Engineering*, 53:263–277, 2018. doi: 10.1016/j.precisioneng.2018.04.008.

[68] A. Susanto, C.-H. Liu, K. Yamada, Y.-R. Hwang, R. Tanaka, and K. Sekiya. Milling process monitoring based on vibration analysis using Hilbert-Huang transform. *International Journal of Automation Technology*, 12(5):688–698, 2018. doi: 10.20965/ijat.2018.p0688.

[69] B. Setiyana, J. Jamari, R. Ismail, and D.J. Schipper. A numerical investigation of the sliding contact between a rigid spherical indenter and a rubber surface: The effect of sliding depth and surface roughness. *Jurnal Tribologi*, 33:20–30, 2022.

[70] B. Setiyana, R. Ismail, J. Jamari, and D.J. Schipper. An analytical study of the wear pattern of an abraded rubber surface: The interaction model. *Tribology – Materilas, Surfaces & Interfaces*, 12(4):186–192, 2018. doi: 10.1080/17515831.2018.1489584.